Available online at www.sciencedirect.com
ScienceDirect
Journal of Magnetic Resonance 182 (2006) 260–272
JMR Journal of Magnetic Resonance
www.elsevier.com/locate/jmr

Auxiliary probe design adaptable to existing probes for remote detection NMR, MRI, and time-of-flight tracing

Songi Han [a,b,*], Josef Granwehr [a,c], Sandra Garcia [a], Erin E. McDonnell [a], Alexander Pines [a]

[a] University of California Berkeley, Department of Chemistry, Lawrence Berkeley National Laboratory, Material Sciences Divisions, Berkeley, CA 94720, USA
[b] University of California Santa Barbara, Department of Chemistry and Biochemistry, Santa Barbara, CA 93111, USA
[c] University of Nottingham, Sir Peter Mansfield Magnetic Resonance Centre, Nottingham NG7 2RD, UK

Received 4 March 2006; revised 9 June 2006
Available online 27 July 2006

Abstract

A versatile, detection-only probe design is presented that can be adapted to any existing NMR or MRI probe with the purpose of making the remote detection concept generally applicable. Remote detection suggests freeing the NMR experiment from the confinement of using the same radio frequency (RF) coil and magnetic field for both information encoding and signal detection. Information is stored during the encoding step onto a fluid sensor medium whose magnetization is later measured in a different location. The choice of an RF probe and magnetic field for encoding can be made based solely on the size and characteristics of the sample and the desired information quality without considering detection sensitivity, as this aspect is dealt with by a separate detector. While early experiments required building probes that included two resonant circuits, one for encoding and one for detection, a modular approach with a detection-only probe as presented here can be used along with any existing NMR probe of choice for encoding. The design of two different detection-only probes is presented, one with a saddle coil for milliliter-sized detection volumes, and the other one with a microsolenoid coil for sub-microliter fluid quantities. As example applications, we present time-of-flight (TOF) tracing of hyperpolarized ^{129}Xe spins in a gas mixture through coiled tubing using the microsolenoid coil detector and TOF flow imaging through a nested glass container where the gas flow changes its direction twice between inlet and outlet using the saddle coil detector.

Keywords: NMR; MRI; Remote detection; Probe design; Flow; Time-of-flight; Sensitivity

1. Introduction

Remote detection NMR or MRI denominates the concept of spatially and temporally separating the encoding and the detection step of an NMR or an MRI experiment [1]. The longitudinal spin magnetization of a fluid is used to store and transport information about an encoding environment or the fluid itself in this particular environment between the two locations. After the encoding step, the fluid is physically relocated to the detector, where its spin magnetization is read out. The encoding step can be any pulse sequence that alters the magnetization of the fluid in a defined way, and therefore the encoded information can be any property accessible with an NMR experiment, for example a spectrum, an image, relaxation times, diffusion constants, or flow velocity. However, with remote detection, each encoding step stores only one data point onto the fluid magnetization in a particular volume element. As a result, the information contained in the precession of transverse magnetization must be sampled point-by-point in subsequent encoding steps. The situation is different if instead of the evolving transverse magnetization, the flow trace of the encoded fluid volume is of interest. The latter can be measured transiently for each encoding step as the fluid arrives at the detector, which

* Corresponding author. Fax: +1 805 893 4120.
E-mail address: songi@chem.ucsb.edu (S. Han).

1090-7807/$ - see front matter © 2006 Elsevier Inc. All rights reserved.
doi:10.1016/j.jmr.2006.06.024

defines a new class of time-of-flight (TOF) experiments for direct flow tracing and characterization [2].

The information-bearing spins can be contained in the analyte of interest, e.g., the ^{1}H of a solvent or ^{13}C of the molecules of interest, or in external, inert tracer atoms like ^{129}Xe admixed to the sample fluid. In any of the cases, the longitudinal magnetization must not fully relax during the time it takes the fluid to travel from the encoding to the detection location. As will be discussed later, longitudinal relaxation of the encoded spins during the time of travel will reduce the sensitivity of the remotely detected signal accordingly.

The separation of the signal detection from the sample location allows the optimization of the NMR encoding environment without compromising on sample size and information quality for the sake of detection sensitivity. Signal read-out can be done by any method capable of sensitively measuring the magnetization of the information-bearing spins. For example, it can be inductive detection using an RF coil, which is favorable at high magnetic fields. It can be a magnetometer like a Superconducting Quantum Interference Device (SQUID) [3] or an atomic magnetometer [4,5] which scale favorably towards low detection fields. Additionally, it can be a method specific to a certain fluid, like spin-exchange optical detection [6] in the case of ^{129}Xe or ^{3}He noble gases. Note that continuous wave RF detection can be used as well without significant sensitivity drawbacks in situations where the fluid has only a single line whose position is known in advance [7]. In experiments where the spectral information in the detection environment is not utilized and no time-resolved detection is desired, the sensitivity can be enhanced by minimizing the detection bandwidth, for example by using multiple echo detection [8].

From theoretical considerations [9] as well as practical experience, three situations are especially suitable for sensitivity enhancement by remote detection. The first case is if sensitive detection is not possible in a particular encoding environment, for example when doing imaging experiments at very low magnetic fields. A remote MRI experiment has been done at an encoding field of 4 mT, where direct inductive detection would not have provided sufficient sensitivity, and signal detection at a magnetic field of 4 T [1]. The second case is NMR and MRI experiments in an environment with short transverse relaxation times, especially if the magnetization cannot be refocused. This is an often occurring problem with samples that have strong internal susceptibility gradients like porous minerals [2]. Remote detection can then be conducted in a separate location with no significant susceptibility gradients. Even in cases where the signal dephasing time is too short to allow for phase-encoding, it is still possible to reconstruct image projections by saturating the magnetization at the sample location with slice-selective pulses and trace their spatial location from the remotely measured signal. And the third case affects samples that either have a low porosity [10] or contain small channels in an otherwise bulky object, so the void space containing the signal-inducing fluid and therefore the filling factor is low. Examples are microfluidic chip devices for handling of fluids in the nanoliter range [11,12]. These chips usually have dimensions on the order of centimeters, while the channels are in the micron range, so that microcoils are required to achieve enough sensitivity per volume in NMR experiments [13,14]. While conventionally NMR was done using small surface coils, or the chips were modified to accommodate a microcoil at a specific location, remote detection allows the use of an imaging probe for signal encoding that houses the whole chip. A microcoil wound around the outlet capillary tubing can then be used for detection [12]. Not only is the use of a large encoding coil convenient as the NMR probe does not have to be custom designed for each chip, but it also opens up new possibilities to study chips of complex three-dimensional geometries in which some channels are not close to the chip's face and therefore not approachable with surface coils.

Apart from sensitivity improvements, remote detection inherently employs fluid flow between the encoding coil and the detector. This flow can itself be studied with a TOF experiment, where the arrival of the fluid at the detector is recorded either transiently or stroboscopically. The TOF dimension can be correlated with the indirect dimensions that are encoded point-by-point to trace the flow field in porous media [2] or microfluidic devices [11] in combination with image encoding sequences, or, by encoding spectral information, to distinguish the flow of different phases by their chemical shift [15].

The first proof of principle experiments at high magnetic fields were done with dedicated home-built probes that accommodated two separate RF coils, one designed for the particular sample of interest to do the NMR encoding, and the other for detection [1,10]. Such an approach requires the construction of a new probe for each type of sample and experiment. For a more general availability of remote detection, an easily adaptable and versatile hardware design is desirable which requires as few custom modifications to an existing setup as possible. We developed for this purpose the concept of an auxiliary, detector-only probe that can be used along with any probe that is adequate for encoding in a particular experiment. We discuss design considerations relevant for this kind of probe and present two different implementations, one optimized for small fluid quantities using a microcoil and the other for universal applicability with larger fluid quantities.

The discussion of sensitivity with remote detection contains two largely different aspects. The first is the theoretical sensitivity enhancement afforded by a particular combination of encoding probe and remote detector, which is best expressed by the signal-to-noise ratio (SNR) in an identical test experiment with both probes. The second aspect is the actual sensitivity enhancement obtained in a real experiment, which not only depends on the comparison between the SNR of both probes, but also the timing of the data acquisition, the flow properties of the sensor

fluid, and the longitudinal relaxation times of the spins contained in this fluid [9]. A balanced discussion in this case is possible using the SNR per square root time as the relevant quantity [7]. We summarize the relevant aspects of a sensitivity discussion for comparing direct and remote detection, with the focus on assessing different probes.

2. Probe design

The probe design principles discussed here are specific for encoding and detection in the same magnetic field. Although remote detection NMR is not confined to using the same magnet for encoding and detection, such a setup has many practical applications [2,10–12,15]. Especially at high magnetic fields, many sophisticated probes for various tasks are readily available. Rebuilding all these probes for use with remote detection by integrating a second RF circuit would be a tedious task that would certainly prevent many researchers from considering this approach. Also, it is not trivial within a series of home-built probes to reproduce features such as multiple channels including a field-frequency lock channel, temperature control, and built-in field gradients, which are available in many commercial probes. However, the feature list for an optimal detection circuit is much less extensive. As most probes designed for liquid-state experiments or for imaging have open access at least from one side, it is inviting to design a separate probe only for detection to be used simultaneously with a conventional probe that is then used only for encoding. Such an auxiliary, detection-only probe can be mounted right at the open front of the existing probe (Fig. 1). As this would block the free sample access to the encoding probe, the detection probe needs to include a mechanism to hold the sample and the flow tubing, which is then inserted into the magnet together with the detection probe. The detection coil needs to be as close to the front of the probe as possible to allow the two coils to be close to each other. This is necessary as both RF coils need to be accommodated within the sweet spot of the same magnet, since outside this sweet spot the field falls off very rapidly. Furthermore, by placing the two coils close to each other, unwanted fluid dispersion between the encoding and the detection step can be minimized, and fluctuations of the flow rate add less noise to the encoded signal [9].

Most high-resolution probes have no space for access inside the probe body. In this case, the detector-only probe has to be placed from the top of the magnet, and the tubing or glassware that pipes the fluid and either contains the stationary sample or is connected to it has to be designed such that the fluid can enter and exit from the same side. Alternatively, microimaging probes with a clear bore facilitate the insertion of the detection probe as well as the flow tubing either from top or from underneath and also allow the placement of the two coils at an almost arbitrary distance from each other. Figs. 1a and b show schematics of both setups.

As the encoding step addresses the same nucleus that will ultimately be detected, care has to be taken to adequately decouple the encoding and detection RF coils, which must be tuned to the same resonance frequency. Significant cross-talk between them would not only increase the noise level, but each detection pulse would also induce a pulse on the encoding coil, causing artifacts that are difficult to handle. The most basic measures to avoid cross-talk are to insert an RF shield and to orient the two coils perpendicular to each other to minimize an overlap between their respective RF fields. In most cases it is simpler to encase the detection coil in a shield, as this is usually the smaller of the two coils and because disturbances of the B_1 field to a certain degree caused by the shield are more acceptable for detection than they would be for encoding. However, it is generally necessary to compromise somewhat on the shield as well, as there must be some tubing connecting the active volumes inside the two coils for the fluid, which typically requires the shield to be pierced. This problem becomes more pronounced with higher RF frequencies, bigger coils, and larger tubing. If a shield is not sufficient to decouple the two coils, one could additionally employ active methods like a Q switch that reduces the quality factor, Q, of the detection circuit during encoding, and the Q of the encoding circuit during detection [17]. The usual problem of inducing additional ringing by the switching is not of major importance here, since the encoding and the detection pulses are separated in time, and switching can be done well before a pulse is applied. Also, care has to be taken that each circuit is properly grounded to avoid current loops that couple the two circuits. The proximity of the detection probe to the encoding volume can lead to additional artifacts if eddy currents are induced in the RF shields around the detector coil by fast switched, high amplitude gradients. However, the cylindrical copper shield that encloses the saddle-coil detector probe in our setup does not lead to noticeable eddy current artifacts for our experimental conditions. We tested this by comparing 2D spin warp images acquired in the absence and presence of the auxiliary detector probe, where the switching interval and the strength of the employed gradients were comparable to our remote detection experiments, and found that the images were indistinguishable (Fig. 2).

As remote detection necessarily involves fluid flow, one must pay special attention to avoid mechanical instabilities of the probes, which affects the reproducibility of an experiment (t_1 noise) [9]. Two different approaches are used in the following to suppress such problems. The first uses a coil that has a larger inner diameter than the outer diameter of the tubing that pipes the fluid from the encoding coil to the detector. In this case the tubing never touches the coil or any supporting structure of the coil. The filling factor of the fluid is not optimal, but small vibrations of the tubing are not immediately transferred to the coil. The second option uses tubing that is rigidly mounted on either side of the detection coil and therefore can serve as a mount for the coil, which is wrapped directly onto the tubing.

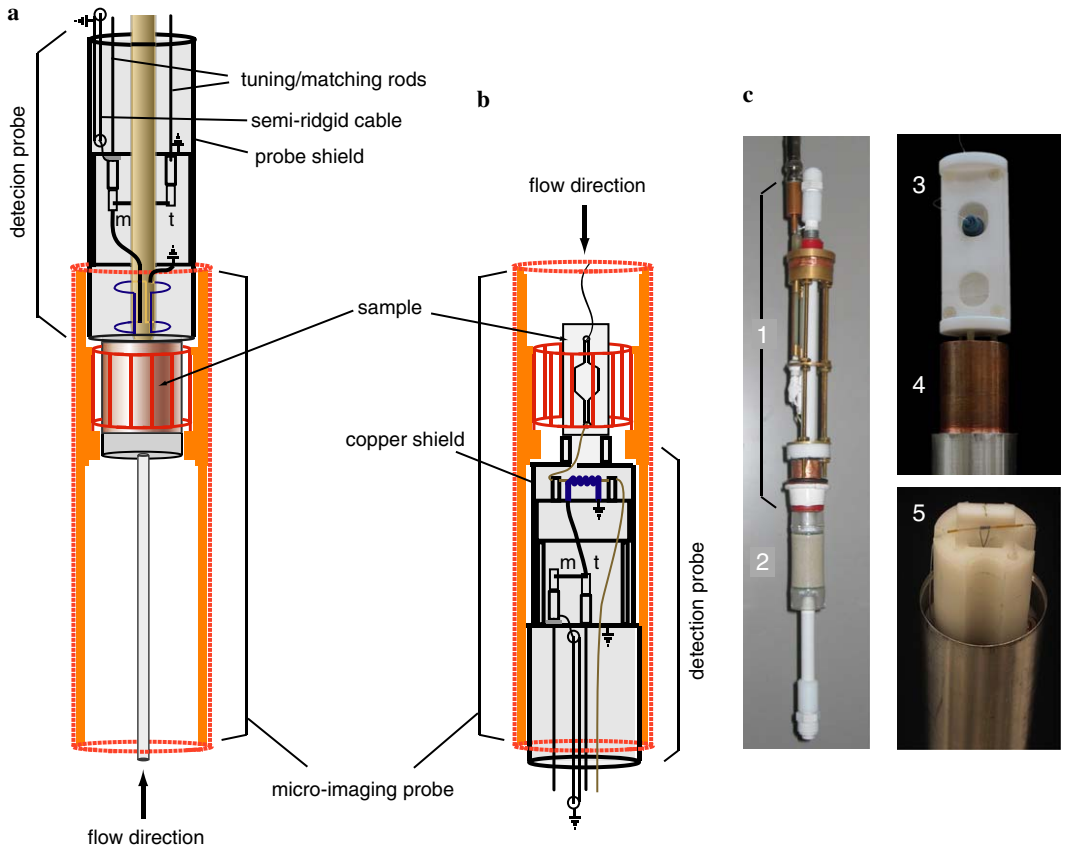

Fig. 1. Schematics of detection-only probes. (a) Sketch of a detection-only probe that contains a saddle coil, allowing the use of straight flow tubing to connect the outlet of the sample and the detection volume. The detection probe is mounted on top of a microimaging probe with an end-to-end bore, which is used for encoding. (b) Sketch of a detection-only probe that contains a microsolenoid coil. This probe is inserted from the bottom into a micro-imaging probe. On top of the detection probe, inside the encoding coil, a microfluidic chip device is mounted. (c) The left photo shows a detection-only probe (1) together with a packed sandstone sample (2). This sandstone was attached to the flow tubing. Probe and sample were inserted from the top into the imaging probe. The upper photo on the right shows a microchannel sample (3) that was mounted in a Teflon frame on the copper shield of a detection probe (4). This assembly is inserted from the bottom into the microimaging probe. The lower photo shows the same probe with the copper head removed, exposing the microcoil and its mounts. Not shown are the two Teflon blocks that are used to stabilize the coil during an experiment.

In this case, the filling factor and therefore the sensitivity is optimized, however the flexibility is compromised as it is not as straightforward to switch the tubing in order to change the diameter of the flow channel.

The effect of instabilities of the tuning and matching on the transfer function of the detection circuit increases with its Q. Such instabilities can originate from vibrations of the coil as well as a change of the sample impedance, caused for example by instabilities of the flow due to bubbles or pressure fluctuations. Slightly lowering the Q or overcoupling the detection circuit can help to reduce this type of noise.

3. Sensitivity discussion

An established measure for sensitivity, which includes the total time required to encode and detect the desired information, is defined as the signal-to-noise ratio (SNR) per square root time, $s/(\sigma_n\sqrt{t_{\mathrm{pt}}})$. $s = m_0 V_0$ is the signal amplitude, where m_0 is the net magnetic moment of all the spins in the detection volume contributing to the signal, and V_0 is the detector-dependent signal per unit magnetic moment. $\sigma_n = \sqrt{\Delta f}\rho_n$ is the r.m.s. noise amplitude, where Δf is the detection bandwidth and ρ_n is the square root of the frequency-independent power spectral density of the thermal noise [7]. We will use the time to acquire one encoded data point, t_{pt}, as the reference time duration, which has the advantage that only a minimum of assumptions regarding the encoding sequence must be made. This is because a single, directly detected data point can be, without further processing, compared with the corresponding encoded data point using remote detection. Superscripts d and r are used for the following equations to distinguish between the parameters in an experiment with direct, transient detection and remote detection, respectively.

To characterize the sensitivity of a particular detector, the quantity V_0/ρ_n, which is independent of experimental parameters, is used. For sensitivity comparison, a test experiment is used that consists of a hard $\pi/2$ pulse and a subsequent free induction decay (FID) that is divided into M equally spaced data points between 0 and $t_{\mathrm{aq}}^{\mathrm{d}}$, recorded

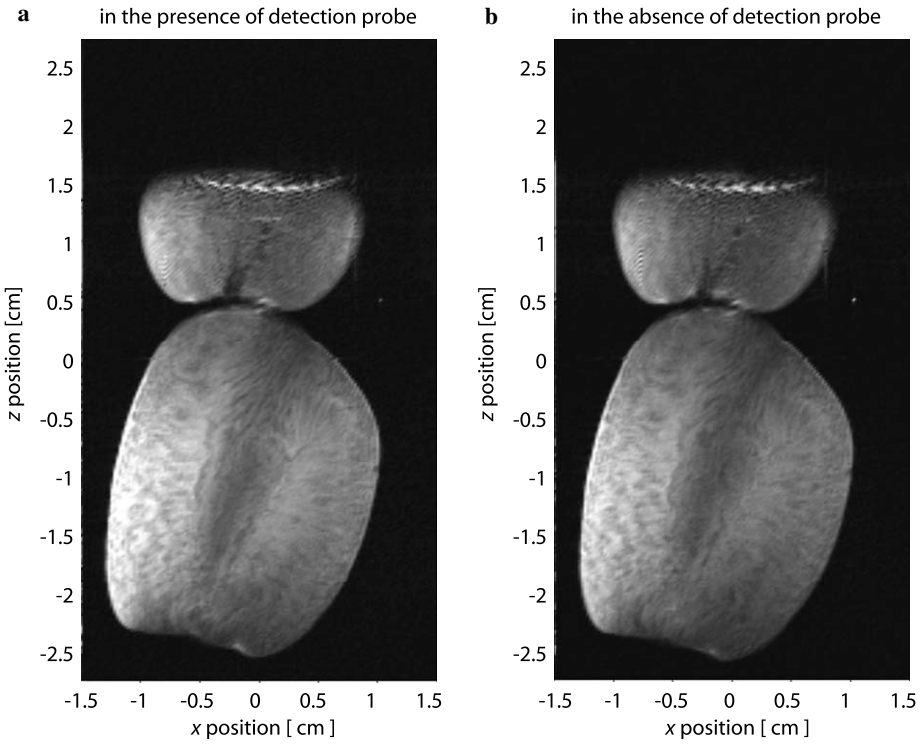

Fig. 2. 2D spin-warp images of grapes using a commercial imaging probe in the absence (a) and presence (b) of the auxiliary, saddle-coil detector probe to determine whether the close proximity of the imaging and the remote probe has an influence on the image quality (details about the probes are described in the experimental section). A *xz*-cross sectional image with 2 mm slice thickness along the *y* direction is acquired, where *z* is the vertical direction and *x*, *y* the horizontal directions. A field of view of 55 mm and 256 pixel along the *z* direction, and a field of view of 30 mm and 128 pixel along the *x* direction were chosen. The image artifacts appearing at the upper edge along the *z* direction in both images are due to B_1 inhomogeneities at the coil rim of the imaging probe.

with quadrature detection, on a sample exhibiting a single line. In an experiment with direct, transient detection, M data points are recorded during each repetition of the experiment, therefore the time to record one data point is the interval between subsequent repetitions of the experiment, $t^{\mathrm{r}}_{\mathrm{rep}}$, divided by M, $t^{\mathrm{d}}_{\mathrm{pt}} = t^{\mathrm{d}}_{\mathrm{rep}}/M$. As detailed in [7], one usually sets $\Delta f^{\mathrm{d}} = M/t^{\mathrm{d}}_{\mathrm{aq}}$, which is the inverse of the dwell time of the data acquisition, and then the sensitivity can be described by

$$\text{sensitivity}^{\mathrm{d}} = \frac{s^{\mathrm{d}}/\rho^{\mathrm{d}}_n}{\sqrt{M/t^{\mathrm{d}}_{\mathrm{aq}}}\sqrt{t^{\mathrm{d}}_{\mathrm{rep}}/M}} = \frac{m^{\mathrm{d}}_0 V^{\mathrm{d}}_0/\rho^{\mathrm{d}}_n}{\sqrt{t^{\mathrm{d}}_{\mathrm{rep}}/t_{\mathrm{aq}}}^{\mathrm{d}}}. \quad (1)$$

To detect the same data point remotely, the transverse magnetization must first be stored as longitudinal magnetization with a $\pi/2$ pulse, then the fluid has to flow to the detector, where its longitudinal magnetization containing the encoded information is read out. Only one data point is encoded with each repetition of the experiment, thus $t^{\mathrm{r}}_{\mathrm{pt}} = t^{\mathrm{r}}_{\mathrm{rep}}$. With inductive detection at high field, remote detection is typically done with a $\pi/2$ pulse and subsequent recording of the FID on the detection circuit, and the signal is obtained as the peak amplitude, S^{r}, after Fourier transform of the FID. The SNR is simply the ratio of S^{r} and the off-resonant noise in this spectrum, $\sigma^{\mathrm{r}}_{\mathrm{N}}$. The bandwidth that determines the noise can be made much narrower with remote detection than with direct, transient detection. If the purpose of the detection step is to measure the total magnetization of the spins in the detection volume without considering any spectral information, the sensitivity of the remote detection step can be optimized with a matched weighting function, where the signal is multiplied with its own envelope. This gives a filter time constant of $T^{\mathrm{r}}_2/2$ instead of the dwell time, and a bandwidth in the frequency domain of $\Delta F^{\mathrm{r}} = 2/T^{\mathrm{r}}_2$. The SNR in the frequency domain is equal to the SNR in the time domain if the data is recorded with the same bandwidth, $\Delta f^{\mathrm{r}} = 2/T^{\mathrm{r}}_2$. To perform the sensitivity discussion in the time domain helps later to define a simple procedure of rating the relative SNR of remote versus encoding probe.

Because remote detection is a point-by-point detection method, only one phase component of the transverse magnetization is stored at the end of each encoding step. In order to obtain a complex data point, each encoding step has to be performed twice, the second time with a storage pulse that is phase shifted by 90° compared to the first one. This effectively doubles the duration of an experiment with remote detection, and therefore reduces the relative sensitivity compared to the direct experiment by a factor $\sqrt{2}$.

Other factors influencing the sensitivity with remote detection include the longitudinal relaxation of the spin magnetization of the sensor fluid during flow and the dilution of encoded with unencoded fluid. Both of these effects

cause m_0^r to be reduced compared to m_0^d. A relaxation term can be introduced as $\varphi = \exp(-t_{trav}/T_1^r)$, where t_{trav} is the time it takes the fluid to travel from the encoding to the detection coil, and T_1^r is the longitudinal relaxation time of the sensor fluid in the tubing that connects the encoding and the detection volume. Longitudinal relaxation in both the encoding and detection coils can occur at different rates, so that the fluid in the outlet of the encoding region will relax for a different time than the fluid that has to cross the entire encoding region. A quantitative discussion depends on the fluid and the sample to be studied [9], but this is not considered here.

When discussing the sensitivity of remote detection, it is also important to consider the relationship between the flow pattern and the flow dispersion during the travel time, as these cause dilution of the encoded spins and therefore influence the optimum choice of detection intervals. The flow dispersion of the encoded spin volume along the main flow direction is much larger for laminar, parabolic flow than for turbulent, plug-like flow. While for parabolic flow, the average flow velocity is at 50% of the maximum flow velocity amplitude occurring at the center of the tube, for plug flow pattern this average lies at 77–87% of the maximum velocity. The latter results in significantly smaller dispersion of the encoded fluid along the flow direction, and therefore the encoded spins are replenished faster within the detector. To simply quantify the sensitivity, a dilution factor ϕ can be defined as the fraction of encoded fluid in the detection volume. The effect of dilution on sensitivity can be minimized by adjusting the detection volume to the volume of the diluted encoded fluid volume, i.e. multiplying the detection volume by ϕ^{-1}. Here, we simply assume that the detection volume is matched to the volume of the encoded fluid, and then m_0^r is scaled by $\phi < 1$ to finally become $m_0^r = \varphi\phi m_0^d$, where also the relaxation term φ is taken into account. The sensitivity with remote detection is then

$$\text{sensitivity}^r = \frac{s^r/\rho_n^r}{\sqrt{2/T_2^r}}\sqrt{2t_{rep}^r} = \frac{\varphi\phi m_0^d V_0^r/\rho_n^r}{\sqrt{2}\sqrt{2t_{rep}^r/T_2^r}}. \quad (2)$$

Not considered in this expression is the higher susceptibility of remote detection to multiplicative or t_1 noise, which affects the reproducibility of an experiment [21]. The fact that multiplicative noise is proportional to the signal results in an upper limit for the SNR with remote detection. Once this SNR is reached, increasing m_0, for example by a better pre-polarization of the sensor fluid, does not change the sensitivity anymore as long as the source of the t_1 noise is not reduced. Particularly the presence of fluctuations of the fluid flow rate causes a capping of the achievable sensitivity, and increasing m_0 in fact reduces the sensitivity enhancement of remote detection [7]. However, this type of noise does not change the potential sensitivity enhancement with remote detection when working at the detection limit of the probes. Therefore, it is not considered in the following discussion which attempts to quantify the relative sensitivity at the limit of a very low SNR with direct detection.

Using Eqs. (1) and (2), the sensitivity of remote versus direct detection compares as

$$\frac{\text{sensitivity}^r}{\text{sensitivity}^d} = \frac{s^r/\rho_n^r}{s^d/\rho_n^d}\sqrt{\frac{t_{rep}^d}{2t_{rep}^r}}\sqrt{\frac{T_2^r}{2t_{aq}^d}} = \frac{\Lambda\varphi\phi}{\sqrt{2}}\sqrt{\frac{t_{rep}^d T_2^r}{2t_{rep}^r t_{aq}^d}}. \quad (3)$$

This equation includes the ratio of the absolute sensitivity of the detector to that of the encoding coil, $\Lambda = (V_0^r/\rho_n^r)/(V_0^d/\rho_n^d)$, the previously discussed dilution of magnetic moments due to relaxation and flow dispersion, the bandwidth, the experimental time and the fact that two acquisitions are needed in order to obtain a complex data point with remote detection. This shows that the sensitivity enhancement of remote detection compared to direct detection is usually less than the factor given by the detector dependent term Λ. However, Λ is the one term in Eq. (3) that includes only properties of the two detectors that are to be compared, while none of the other terms are dependent on the specific detector. Therefore Λ is used to assess the potential sensitivity enhancement of a particular probe combination. This can be determined by comparing both probes using identical test experiments and the same sample. Note that this procedure is only applicable if the signal dephasing time is identical in both probes. If this is not possible to achieve, one can compare the intensity of the first data point of the FID (or, equivalently, the integrated signal of the spectrum), divided by the respective r.m.s. noise amplitude. If the number of scans for the experiments with the remote and the encoding probe, n^r and n^d respectively, are not equal, the sensitivity of both probes needs to be normalized by dividing the SNR by $\sqrt{n}$. Likewise, if a different sample volume is used in the two probes, the SNR has to be divided by this volume such that the sensitivity of both probes is normalized to the same volume.

With inductive detection, the absolute sensitivity increases with the total number of signal carrying spins, which is typically proportional to the sample volume, while the SNR per unit volume decreases with the square root of the coil volume (V_c) or linearly with the coil diameter [16], as discussed previously [9,10], if detection frequency, bandwidth and temperature remain the same. The SNR of an LCR tank circuit is proportional to

$$\text{SNR}_{LCR} \propto m_0\sqrt{\frac{Q}{V_c}} \propto m_0 B_1 \propto \frac{m_0}{t_{90}}. \quad (4)$$

The second and third proportionality in Eq. (4) allow for the estimation of SNR from the strength of the RF field (B_1), which is inversely proportional to the $\pi/2$ pulse length, t_{90}, for a given RF power level, in agreement with the principle of reciprocity [16]. This suggests a particularly simple method to determine the relative sensitivity of the two circuits in a remote setup as

$$\Lambda = \frac{V_0^r/\rho_n^r}{V_0^d/\rho_n^d} = \frac{t_{90}^d}{t_{90}^r}. \quad (5)$$

According to the first proportionality in Eq. (4) the main factor to consider when designing a remote detection coil is the optimal detection volume, V_d. The maximum sensitivity is obtained when all the encoded fluid is collected and its magnetization read out in one step. However, during its flow from the encoding to the detection volume, it usually gets partially diluted with unencoded fluid as discussed above. One has to distinguish experiments with homogeneous and inhomogeneous encoding. In the first case, all the fluid in the whole encoding volume is encoded with the same information, while in the second case, spatially variable information is encoded. In the homogeneous case, it is not necessary that the longitudinal magnetization of all the encoded fluid is read out during detection. It is only necessary that the time between subsequent encoding steps is long enough that none of the fluid gets encoded twice to avoid artifacts. Depending on the profile of the fluid flow through the detection volume, it may be advantageous to cut off the leading and the tailing edge of the arriving fluid for optimum sensitivity, as fluctuations in the flow rate have a stronger effect on the detected signal in those regions of the flow curve [9]. On the other hand, if the encoded information is inhomogeneous, all the encoded fluid has to be read out in order to avoid spatial artifacts, even though this may somewhat reduce the sensitivity because there will be some mixing of the encoded with unencoded fluid, and a larger detection volume, V_d, compared to the encoding volume, V_p, is required.

The optimum choice of V_d is more complicated in a TOF experiment. In short, V_d should be matched with the desired time resolution, Δt, which relates to the volumetric flow rate, q, as

$$V_d = \frac{q}{\Delta t}. \tag{6}$$

This assumes that detection is done stroboscopically with a train of detection pulses spaced by Δt. Ideally Δt is adjusted so that all of the fluid within the detection volume gets replaced between subsequent detection pulses, but at the same time no fluid passes the detector without being read out. These two conditions can only be met at the same time for ideal plug flow inside the detector, where the flow velocity is nearly uniform across the tube diameter. If a gas is used, this velocity may be averaged out during Δt if the diffusion across the tubing cross-section is effective, which requires a sufficiently small tubing diameter. To avoid artifacts, especially in imaging experiments, one has to make sure that no encoded fluid passes the detection volume without being read out. Therefore it is usually advisable to select Δt somewhat shorter than q/V_d. If the flip angle of the detection pulse is set carefully to $\pi/2$ and the RF field, B_1, of the detection coil is homogeneous across the detection volume, the errors from spins that experienced two detection pulses is small. But if the fraction of fluid that is replaced between detection pulses is too small, the noise increases disproportionately. As a rule of thumb, Δt should not be shorter than half the average time it takes for the fluid to flow through the detection volume, i.e. $q/2V_d < \Delta t < q/V_d$. This lower limit value can be determined experimentally as the zero crossing in an inversion recovery experiment on the detection coil while the fluid is flowing. As Δt in a TOF experiment is typically short compared to the T_1 of a target nucleus, the measured "recovery time" corresponds in fact to the time it takes to replace the fluid in the detection coil. As long as the sensitivity is good enough that the coil dimensions do not need to be fully optimized, the time resolution can be changed by adjusting the inner diameter of the tube using an inset on the length of the detection coil to reduce V_d. However, in experiments that are operating at the absolute limit of sensitivity [11], the optimized dimensions have to be determined in advance for the flow rate that is to be used.

Another aspect that is primarily of importance with TOF experiments is the type of detection coil to be used. To minimize the impact of the tubing on fluid dispersion between the outlet of the encoding volume and the detector, and to ensure simple sample and probe handling, straight tubing would be desired. But this requires a coil with its field direction perpendicular to its axis such as a saddle coil or a birdcage coil (see Fig. 1a). These coils are not only difficult to make for coil diameters less than 5 mm, but also significantly less sensitive than solenoid coils [16,17]. The latter, however, require a bend in the tubing, as their axis is perpendicular to the bore of the magnet in the case of a common superconducting magnet (see Fig. 1b). Each option was implemented in one of the probes described next.

4. Detection probe with milliliter range detection volume

The first probe built with this modular approach was designed for maximum flexibility, with flow and imaging experiments of porous media in mind. Such materials often show substantial internal field gradients due to the magnetic susceptibility of the solid matrix, causing short transverse dephasing times, which are especially difficult to refocus for gaseous fluids, among others, due to the strong presence of incoherent flow and fast diffusion across the pores that lead to incoherent phase losses. The application of remote detection can permit a sensitivity advantage for such systems of up to an order of magnitude even with equally sensitive encoding and detection coils [9].

The probe employed a saddle-shaped coil that could be used with straight tubing up to 1/2 in. outer diameter without touching the coil (Fig. 1a). This coil was mounted on a cylindrical support (Kel-F plastic) with four grooves carved in parallel to the axis to support the wire. The coil was enclosed by a grounded copper shield to isolate it from the encoding coil. An aluminum tube encased the whole length of the probe and served as a shield for the rest of the circuit. In the present configuration, the upper rim of the encoding coil was about 2.5 cm away from the forefront of the detection coil. This design is adaptable to basically any encoding probe that is open on one side. In addition to this generic design, a support cylinder

(Teflon plastic) that fitted snug on the outside of the aluminum tube of the detection probe and the inner bore of the gradient stack was built according to an inverse imprint of the available space to hold the probe centered and mechanically stable. The sample could be mounted at the end of the tubing right below the detection coil using, for example, a threaded connection (Fig. 1c). Sample and detection probe then could be inserted into the magnet together, after the encoding probe had been mounted inside the magnet independently.

Using variable capacitors (Polyflon, Norwalk, CT), which were placed on a support in the body of the detection probe, the circuit could be tuned over a range of frequencies that covered both ^{129}Xe and ^{13}C nuclei, so that shimming could be done using a stationary ^{13}C-enriched liquid sample instead of ^{129}Xe gas.

5. Detection probe with microliter range detection volume

A second remote detection probe was built for the purpose of optimizing sensitivity of small sample volumes below 1 μl. It was designed specifically to be used with an open-bore microimaging probe, into which it was introduced from the bottom (Fig. 1b). A microsolenoid detection coil was wrapped directly around a supporting polyimide sleeve (Fig. 1c) and additionally stabilized externally by a solid mount to avoid vibrations induced by the flowing fluid. This was done with a holder made of two pieces that, when screwed together, formed a block with a channel having an inner diameter corresponding to the outer diameter of the detection coil. Also, a robust copper head was used as a shield for the coil and as a mechanical brace to stabilize the various parts of the head of the probe including the coil-stabilizing block. The high shielding factor of this head allowed the minimization of the distance from the detection coil to the rim of the encoding coil to about 1 cm. Furthermore, the copper head served as a mount onto which the microdevices could be attached, ensuring good reproducibility of this configuration in repeated runs of an experiment.

A special requirement with microfluidic devices is that fluid reservoirs are to be avoided between the outlet of a device and the detection coil, as they cause additional fluid dispersion that does not contain any information about the sample of interest [11]. Such reservoirs also reduce the sensitivity, particularly in TOF experiments, because they cause additional mixing of encoded and unencoded fluid. Connections that do not provide a smooth transition between the tubing and a device outlet are especially prone to such reservoirs.

6. Results

6.1. Microsolenoid coil detector probe

We present basic remote detection experiments in order to demonstrate the performance of the auxiliary, microsolenoid coil detector probe in combination with a standard, commercial imaging probe. The first experiment was to determine the expected and the actual sensitivity enhancement from remote detection. For ^{129}Xe, t_{90} of the imaging coil was a factor 127 longer than t_{90} of the microsolenoid coil at the same RF power level. Therefore, according to Eq. (5), the probe-dependent part of the sensitivity enhancement was $\Lambda = 127$. To verify this result, the intensities of the directly detected signals using the imaging probe versus the microsolenoid coil probe were compared for the same fluid volume with a continuously flowing carrier fluid. For this purpose a tube with 0.4-mm inner diameter was placed straight through the imaging coil with a length of 40 mm and then through the detection coil with a length of 5 mm. Therefore the fluid volume in the imaging coil (5 μl) was a factor 8 larger than in the detection coil (0.6 μl). Using the imaging coil, a SNR ratio of 8.0 was obtained in an experiment with 10,000 scans and a total acquisition time of 53 min. To determine the SNR, an exponential apodization function corresponding to a linewidth of 200 Hz was used to minimize the effect of different signal decay times in the two coils. Especially in the microsolenoid coil, this decay time is largely determined by the outflow time of the fluid from the coil, which is different from the signal decay time in the imaging coil. Using the microsolenoid coil, the SNR was 6.9 when 16 scans were co-added taking 5 s for the total acquisition. When comparing the SNR per square root of the number of scans for a given fluid volume, the detector sensitivity was found to be better by a factor $\Lambda = 176$. The discrepancy from the value obtained through measuring the t_{90} ratio may be because of the large error in determining the SNR of the experiments using both probes and the uncertainty in determining the length of the microcoil to only one significant digit.

The same experiment was performed with remote detection, where encoding was done using the imaging probe and detection was done with the microsolenoid probe. The remotely detected spectrum was acquired using 16 scans and 128 points along the encoding dimension within a total experimental time of 8 min, yielding a SNR of 15 for a 0.6 μl volume of hyperpolarized ^{129}Xe gas. Therefore, if equal volumes are compared, the total SNR gain per square root of experimental time amounts to 39-fold with remote detection (Fig. 3a). The discrepancy between this value and the detector dependent sensitivity gain, Λ, reflects the influence of the different parameters in Eq. (3) on the sensitivity enhancement. While φ and ϕ both were close to unity and $t^{d}_{rep} \approx t^{r}_{rep}$, T^{r}_{2} was significantly shorter than t^{d}_{aq}. In addition, fluctuations of the flow rate during the time course of the experiment, which introduce multiplicative noise, can significantly diminish the sensitivity. This can be quantified by comparing the noise level of the remotely detected spectrum with the noise level of a single acquisition with the remote probe. If the two noise levels are not identical, the difference can be accounted for by multiplicative noise. In our setup, the noise level of the

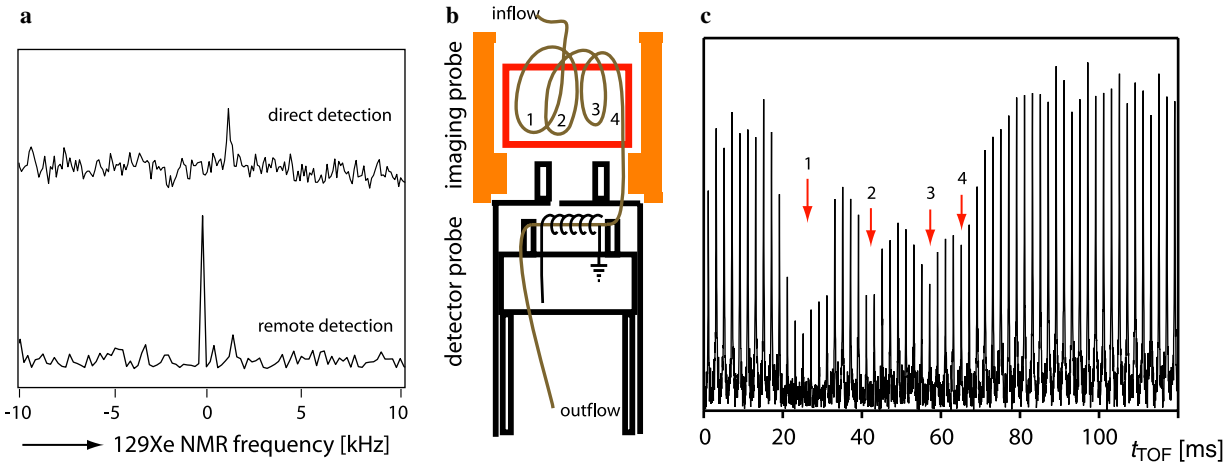

Fig. 3. The performance of the ^{129}Xe microsolenoid detector probe was tested by 1D remote detection spectroscopy and 1D time-of-flight tracing, where information was encoded in the commercial imaging probe. (a) Comparison of 1D ^{129}Xe NMR spectra encoded in the imaging probe and directly detected with the imaging probe (top) versus remotely detected with the microsolenoid coil (bottom). A 39-fold sensitivity enhancement was obtained per same spin volume with remote detection. (b and c) 1D time-of-flight tracing of ^{129}Xe spins that were inverted in the imaging probe. (b) Schematic experimental setup, where spiraled tubing with 0.8 mm inner diameter was placed in the large imaging coil and subsequently fed through the microsolenoid coil. The tubing was twisted into three loops and placed in the imaging coil so that the upper part of the tubing lied outside the imaging coil region. The dips in the travel time curve in (c), labeled with numbers 1–4, were caused by spins that were located inside the imaging probe during the encoding step, and therefore their magnetization was inverted. However, the measured signal does not get inverted due to mixing of the encoded with unencoded spins.

remotely detected spectrum was about 2-fold higher compared to the directly detected spectrum using the remote detector, indicating that multiplicative noise contributed significantly to the reduced sensitivity gain by remote detection.

The next basic experiment was a 1D TOF flow tracing of inverted ^{129}Xe spins as they travel from the imaging probe through 0.8 mm inner diameter plastic tubing to the detector probe, where a coil of 2 mm inner diameter was used. The tubing was coiled into three loops and placed inside the imaging coil such that part of the loops were located outside the resonator as indicated in the sketch of Fig. 3b. A series of 60 detection pulses with 2 ms intervals was applied. This resulted in a characteristic travel time curve with four local minima and three local maxima (Fig. 3c) because only the spins located inside the RF coil of the imaging probe at the time of encoding were inverted by the π pulse applied at $t_{TOF} = 0$ with the encoding coil. The reason why we do not observe inverted spins at the detector is due to significant mixing of the encoded (i.e. inverted) with unencoded spins, which most likely can be attributed to incoherent flow patterns that can be caused by liquid holdup or flow rate fluctuations.

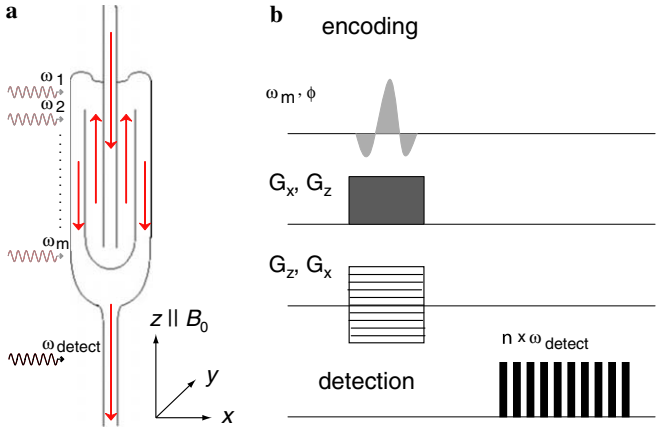

Fig. 4. (a) Cross-section of the cylindrical phantom containing connected chambers that lead the fluid along a curved pathway from the inlet to the outlet. (b) Pulse scheme of a TOF remote experiment. The spin magnetization is inverted slice-selectively during encoding by applying a selective RF pulse in the presence of a field gradient (G_x, G_z). Detection is done stroboscopically by applying a train of π/2 RF pulses as the fluid flows out of the phantom. The inverted spins can be tracked by monitoring their arrival at the detection location as a function of the encoding location, which can be varied by changing the carrier frequency, ω_m, of the RF pulse.

6.2. Saddle coil detector probe

As an example experiment for a saddle coil probe setup, a TOF experiment to visualize gas flow through a glass vessel with cylindrical symmetry is presented, where a fluid has to change its direction twice as it flows from the inlet to the outlet. A side view of this object is shown in Fig. 4a. The fluid flow can be traced by inverting the spin magnetization in a specific volume inside the encoding coil and recording the arrival of these tagged spins at the detection location. As the arrival of the encoded fluid in the detector depends on its flow path through the object, the detailed trace of the flowing spins from any given slice or volume element can be directly visualized if proper slice selection and/or phase-encoding imaging techniques are combined with stroboscopic detection [2]. This experimental approach to measure hydrodynamic dispersion is similar to the technique of an initial narrow-pulse tracer injection, with the

subsequent observation of the effluent concentration of the tracer [18,19]. The difference is that using MRI techniques the "point of injection" can be defined non-invasively anywhere inside the porous medium. Equally important is that the spin magnetization behaves like an ideal tracer, as it does not affect the properties of the flowing medium.

A simple pulse sequence is shown in Fig. 4b. A selective π-pulse in the presence of a linear field gradient inverts the ^{129}Xe spin magnetization within a slice of given thickness and position in the sample. The fluid present in this slice during the encoding step then travels through the object to the detector, where the arrival of the encoded spins cause a drop in spin magnetization, which is continuously monitored by repeatedly applying π/2 detection pulses and subsequent recording of the free induction decay (FID). The amplitude difference between each FID and the signal measured without applying an encoding sequence is proportional to the amount of encoded fluid in the detection volume. The thickness Δr of the encoded slice is given by $\Delta r = \Delta\omega/\gamma G_n$, where $\Delta\omega$ is the excitation bandwidth of the selective pulse, γ is the gyromagnetic ratio of the target nucleus, and G_n is the amplitude of the field gradient. The slice position r_n relative to the center of the gradient coil is determined by $r_n = (\omega_m - \omega_0)/\gamma G_n$, where ω_m is the carrier frequency of the selective RF pulse and ω_0 is the resonance frequency of the target nucleus in the absence of a field gradient. As indicated in the sketch of the flow vessel in Fig. 4a, different slices may be selected by changing ω_m in the presence of a constant field gradient.

Fig. 5 shows the results of two TOF experiments with slice-selective encoding. Slices either parallel or perpendicular to the flow direction (z) were inverted during encoding (Fig. 5a). The position of the slice was moved across the whole sample along the indirect dimension of the experiment. The detection pulses were spaced by $\Delta t = 100$ ms intervals. Each slice was recorded four times, with the position of the detection pulses shifted by 25 ms between subsequent experiments. This interleaved data acquisition allowed for a smoother representation of the TOF data and corresponds to signal averaging, but as long as the time between detection pulses is not longer than the time it takes the sensor medium to flow through the detection volume, the temporal resolution is not improved. The mean arrival time of the spins at the detector and their dispersion depend on the flow profile, the flow path, and the flow distance of the fluid. They therefore depend on the material and the geometry of the stationary object as well as on the viscosity and diffusivity of the fluid.

Contour plots of TOF measurements are shown in Fig. 5b. The upper graph of Fig. 5b depicts the result of an experiment with slices selected parallel to the flow direction. The flow trace through the innermost tube, which lies closest to the outlet and therefore contains spin packets flowing out most quickly, is nicely visible as a dark spot in the slice through the center of the x cross section. Spins flowing through the next outer ring are slower because the cross-sectional area increases, while the mass flow rate is constant. The flow curve at different positions of x show how slices below and above the center contain, as expected, spins with later arrival times around 0.5–2.5 s. The spins with arrival times >3 s originate from the outermost ring.

The two main characteristics of the flow profiles are the average arrival time of the fluid and its spread or dispersion. The longer the time between encoding and detection is, the stronger are the influence of diffusion and the distribution of local flow velocities, causing the spreading

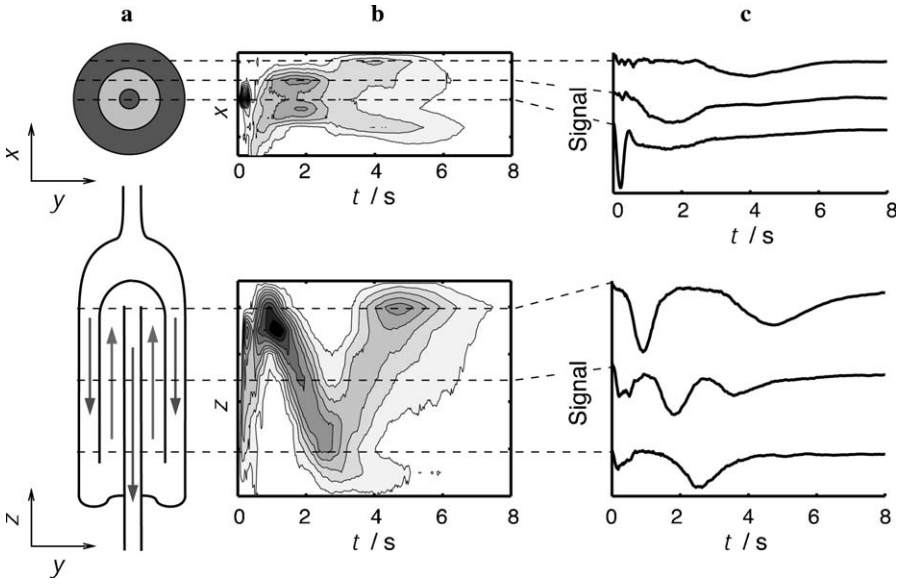

Fig. 5. Time-of-flight vs. encoding position of gas flowing through a cylindrically symmetric glass phantom with large "pores" on the order of 1 cm diameter, obtained with slice selective inversion of magnetization. The flow direction changes twice as the gas is flowing from inlet to outlet. Slices parallel (upper) and perpendicular (lower) to the flow direction were inverted. (a) Cross-section of the object perpendicular to the inverted slices. The arrows in the lower graph depict the direction of the gas flow. (b) Contour plots of the signal. (c) TOF signal of selected slices, as indicated by the dashed lines.

of the arrival time. This broadening is also caused by the acceleration of the gas as it switches over from a wider into a narrower compartment of the glass object. The lower graph of Fig. 5b shows the outflow pattern when slices perpendicular to the flow direction were inverted. The three straight patterns with two sign changes of the slope represent the tube flow that changes it direction twice because three counter-flowing streams are neighboring. Note that if a spatial dimension is plotted vs. TOF the slope of the flow profile represents the flow velocity in the direction normal to the plane of the slices. If a material with unknown pore structure is analyzed, this mean flow velocity allows to determine the local effective porosity, which characterizes the fraction of well connected pores through which the fluid is flowing relative to the total volume of the porous medium [18,20]. The slope in the upper graph of Fig. 5b, where slices parallel to the flow direction are traced, is only non-zero, i.e. has a lateral component, at the points of inflection of the flow.

Hydrodynamic dispersion causes an initially narrow slice of encoded spins to broaden, but the total number of encoded spins remains constant. Therefore as the dispersion pattern gets broader, it also gets less intensive. If dispersion is strong, this may finally limit the time scale of a TOF experiment when the signal decays below the noise level. Another consequence of the decreasing signal intensity is that contour plots as used in Fig. 5b may be misleading, because they tend to suppress the width of a pattern if at the same time its intensity is reduced. To avoid this, the one-dimensional TOF trace of a particular encoding step is a better representation to analyze dispersion (Fig. 5c). In the lower graph of Fig. 5c, one can see the arrival of fluid from different compartments of the fluid vessel. All travel time curves taken from different slices throughout the sample show multiple minima at different arrival times, up to three corresponding to the three counter flowing fluid compartments. Note that interpretation of dispersion becomes complicated as soon as there is more than one flow path for the fluid. This can be seen in the lower graph of Fig. 5b at an arrival time of about 4 s when the pattern splits in two branches. One branch corresponds to gas that flows coherently from the outer into the middle compartment, and the other corresponds to gas that remains stationary for a while at the bottom of the loop and exchanges only gradually with gas in the flow stream.

7. Discussion and conclusions

We have presented a versatile hardware approach for the realization of remote detection NMR and MRI experiments using a separate detection-only probe to allow encoding using a standard probe with open access from at least one side. In the presented case, the distance between the two coils is kept as small as possible to fit both coils inside the sweet-spot of a high-field magnet. The close vicinity requires the two coils to be well shielded from each other to avoid cross-talk. For this purpose, it is easier to make a strong shield around the detection coil than to modify the encoding probe to include a better RF shield, because usually the detection coil is smaller and high resolution is not of utmost importance for detection.

It is often not possible to obtain a good shim for the encoding and detection volume at the same time, especially if encoding is done with a microimaging probe whose RF coil fills almost completely the volume of the sweet spot of a typical high-field magnet and standard shim stack. As a result, a compromise must be achieved that is specific to the problem being studied. We typically inserted both the encoding and the detection coil slightly off the center of the sweet spot of the magnet—one of them above and the other below the ideal position. We shimmed a given volume in the encoding probe first. Then the detection probe was shimmed while iteratively monitoring the shim quality at the encoding coil. If higher sensitivity is required, it may be necessary to shim the detection coil more carefully at the expense of a reduced resolution of the encoded information.

We have demonstrated how simple experiments can be used to assess the potential for sensitivity enhancement of a particular combination of encoding and remote detection probe, and which factors must be considered in order to get a balanced comparison. The presented experiments were not carried out under highly optimized conditions, but represent realistic figures that can be expected when microcoil probes are used for the detection of spins that have been encoded using a conventional imaging probe. The ratio of the SNR per unit volume for the two probes represents usually an upper limit for the potential sensitivity enhancement when a spectroscopy experiment is carried out with remote detection. However, even for remote detectors like the presented saddle coil probe without significantly higher sensitivity, remote detection experiments can be greatly beneficial if imaging experiments of fluids in porous media with large internal susceptibility gradients are carried out. This is because the more homogeneous remote detection environment not containing the porous sample leads to a correspondingly longer signal decay time.

We have shown that it is possible to construct probes that can be inserted from the top or the bottom into the magnet for the purpose of NMR and MRI remote detection. Many commercial imaging probes have open bore access to the sample volume so that the detection coil could be placed below the encoding coil. Inserting the detection probe from below provides minimal stress on the sample or sample vessel, while more space for the detection probe is available if it is inserted from above. If the probe does not have a clear bore, as is the case for most liquid-state probes, the detection probe has to be placed above the encoding probe.

Besides demonstrating the general applicability of our detector design with commercial imaging hardware, we also demonstrated the great potential of remote detection for 1D time-of-flight flow tracing and 2D time-of-flight flow imaging, where the transient flow dimension is utilized

to obtain direct representations of the flow velocity and dispersion. This technique is also applicable to samples that cause strong inhomogeneous line broadening, because the detection is done in a location with no significant susceptibility gradients. Even if the transverse relaxation time at the encoding environment is too short to allow for phase-encoding, spins originating from different slices or volume elements can still be tagged and their flow path and dispersion traced, allowing the imaging and tracing of fluid transport through a variety of samples that conventionally have been difficult to access.

8. Experimental

The experiments were performed on a Unity Inova spectrometer (Varian, Palo Alto, CA) with a 7 T superconducting wide-bore magnet (Oxford Instruments, Cambridge UK). An actively shielded microimaging gradient stack (Resonance Research, Billerica, MA) was used that produced pulsed *xyz* field gradients up to 100 G/cm. The encoding and the detection probes were tuned to the frequency of ^{129}Xe (82.92 MHz). For encoding, a two-channel (^{1}H and ^{129}Xe) microimaging probe with a 25 mm diameter sample bore was used (Varian). The $\pi/2$ pulse length of the ^{129}Xe channel of the imaging probe was 140 μs at a given transmitter power—the RF power setting for all experiments presented in this manuscript was equal and amounted to approximately 100 W. The detection probes could be tuned to ^{129}Xe and ^{13}C frequencies. Additionally, the microsolenoid probe could also be used at ^{1}H frequency by exchanging the tuning and matching capacitors [12].

The saddle-coil-based detection-only probe had a coil inner diameter of 16 mm and a length of 25 mm. The quality factor of this probe was measured to be 100, and it had a $\pi/2$ pulse length of 55 μs at the RF power used for the experiments. The microsolenoid-coil-based detection-only probe had a diameter of 36 mm at base, 29 mm at the head, and a length of 560 mm. The microcoil was positioned less than a centimeter below the lower edge of the imaging coil, which corresponds to a distance between the center of the imaging coil and the microcoil of 3 cm. The microsolenoid coil that was used for the sensitivity discussion and the 1D ^{129}Xe remote spectroscopy experiment had an inner diameter of 0.8 mm, and the one used for the 1D time-of-flight experiment had an inner diameter of 2 mm. The quality factor of the 0.8 mm coil probe was measured to be 66, and it had a $\pi/2$ pulse length of 1.1 μs at the RF power of 100 W. The quality factor of the 2 mm coil probe was measured to be 52, and it had a $\pi/2$ pulse length of 2.8 μs at the same RF power.

A Xe:N_2:He (1:10:89) gas mixture (Spectra Gases, Columbia, MD) was used for the experiments. ^{129}Xe, which was present in natural abundance of 26.4% of the total xenon concentration, was hyperpolarized with a commercial polarizer (former MITI, Amersham, Durham, NC) to approximately 10% nuclear spin polarization by spin-exchange optical pumping with rubidium vapor. The experiments were performed in continuous flow mode, and the gas was vented after it passed the detection coil. The pressure was adjusted to about 7 bar in the pumping cell and to 1 bar in the phantom and the detection volume. The flow rate of 0.6 standard-liter-per-minute (slm) was maintained in the flow profiling experiment of the cylindrical glass phantom using a constant pressure differential between the pumping cell and the outlet valve as the driving force. For the microcoil TOF experiment, a flow rate of 1 slm was maintained at the inlet of the pumping cell. For this experiment, the pressure differential between the pumping cell and the location of the detector was much higher than described above because the outflow pressure at the tubing end was not controlled and restricted with a valve. This led to substantial flow rate fluctuations, which explains the large mixing of fluids observed in the features of the 1D TOF result. For the experiments in the sensitivity discussion, the flow rate at the pumping cell was maintained at 1 slm. A flow splitter was then used before the encoding probe inlet to reduce the flow rate of the gas through the microtubing to a value of 0.002 slm, allowing the flow rates in the pumping cell and through the coil to be independently adjusted.

Acknowledgments

We acknowledge Christian Hilty, Juliette Seeley and Rachel Martin whose effort and knowledge contributed to the quality of the probes that are presented in this paper. Adam Moulé designed the glass vessel that was used to demonstrate the function of the detector-only probe and originally suggested basic travel-time type of experiments that can be regarded as a predecessor experiment of the spatially resolved TOF experiments measured by remote detection. This work was supported by the Director, Office of Science, Office of Basic Energy Sciences, Materials Sciences and Nuclear Science Divisions, of the U.S. Department of Energy under contract DE-AC03-76SF00098.

References

[1] A.J. Moulé, M.M. Spence, S. Han, J.A. Seeley, K.L. Pierce, S.K. Saxena, A. Pines, Amplification of xenon NMR and MRI by remote detection, Proc. Natl. Acad. Sci. USA 100 (2003) 9122–9127.
[2] J. Granwehr, E. Harel, S. Han, S. Garcia, A. Pines, Y. Song, P. Sen, Time-of-flight flow imaging using NMR remote detection, Phys. Rev. Lett. 95 (2005) 075503.
[3] R. McDermott, A.H. Trabesinger, M. Mück, E.L. Hahn, A. Pines, J. Clarke, Liquid-state NMR and scalar couplings in microtesla magnetic fields, Science 295 (2002) 2247–2249.
[4] I.K. Kominis, T.W. Kornack, J.C. Allred, M.V. Romalis, A subfemtotesla multichannel atomic magnetometer, Nature 422 (2003) 596–599.
[5] V.V. Yashchuk, J. Granwehr, D.F. Kimball, S.M. Rochester, A.H. Trabesinger, J.T. Urban, D. Budker, A. Pines, Atomic magnetometry for detection of nuclear magnetization, Phys. Rev. Lett. 93 (2004) 160801.
[6] D. Raftery, H. Long, D. Shykind, P.J. Grandinetti, A. Pines, Multiple-pulse nuclear magnetic resonance of optically pumped xenon in a low magnetic field, Phys. Rev. A 50 (1994) 567–574.

[7] R.R. Ernst, G. Bodenhausen, A. Wokaun, Principles of Nuclear Magnetic Resonance in One and Two Dimensions, Oxford, Clarendon Press, 1987.
[8] O.N. Antzutkin, R. Tycko, High-order multiple quantum excitation in 13-C nuclear magnetic resonance spectroscopy of organic solids, J. Chem. Phys. 110 (1999) 2749.
[9] J. Granwehr, J.A. Seeley, Sensitivity quantification of remote detection NMR and MRI, J. Magn. Reson. 179 (2006) 229–238.
[10] J.A. Seeley, S. Han, A. Pines, Remotely detected high-field MRI of porous samples, J. Magn. Reson. 167 (2004) 282–290.
[11] C. Hilty, E. McDonnell, J. Granwehr, K.L. Pierce, S. Han, A. Pines, Microfluidic gas-flow profiling using remote-detection NMR, Proc. Natl. Acad. Sci. USA 102 (2005) 14960–14963.
[12] E. McDonnell, S. Han, C. Hilty, K.L. Pierce, A. Pines, NMR analysis on microfluidic devices by remote detection, Anal. Chem. 77 (2005) 8109–8114.
[13] E.W. McFarland, A. Mortara, Three-dimensional NMR microscopy: improving SNR with temperature and microcoils, Magn. Reson. Imag. 10 (1992) 279–288.
[14] C. Massin, F. Vincent, A. Homsy, K. Ehrmann, G. Boero, P.-A. Besse, A. Daridon, E. Verpoorte, N.F. de Rooij, R.S. Popovic, Planar microcoil-based microfluidic NMR probes, J. Magn. Reson. 164 (2003) 242–255.
[15] E. Harel, J. Granwehr, J.A. Seeley, A. Pines, Multiphase imaging of gas flow in a nanoporous material using remote detection NMR, Nat. Mater. 5 (2006) 243–333.
[16] D.I. Hoult, R.E. Richards, The signal-to-noise ratio of the nuclear magnetic resonance experiment, J. Magn. Reson. 24 (1976) 71–85.
[17] P.K. Grannell, M.J. Orchard, P. Mansfield, A.N. Garroway, D.C. Stalker, A FET analogue switch for pulsed NMR receivers, J. Phys. E 6 (1973) 1202–1204.
[18] J. Bear, Dynamics of Fluids in Porous Media, American Elsevier, New York, 1972.
[19] M.H.G. Amin, S.J. Gibbs, R.J. Chorley, K.S. Richards, T.A. Carpenter, L.D. Hall, Study of flow and hydrodynamic dispersion in a porous medium using pulsed-field-gradient magnetic resonance, Proc. R. Soc. Lond. A 453 (1997) 489–513.
[20] R. Wang, R.W. Mair, M.S. Rosen, D.G. Cory, R.L. Walsworth, Simultaneous measurement of rock permeability and effective porosity using laser-polarized noble gas NMR, Phys. Rev. E 70 (2004) 026312–026318.
[21] A.F. Mehlkopf, D. Korbee, T.A. Tiggelman, R. Freeman, Sources of t_1 noise in two-dimensional NMR, J. Magn. Reson. 58 (1984) 315–323.